1775

JPn

Neuroscience

The Journal of Physiology

Causal relationships between neurons of the nucleus incertus and the hippocampal theta activity in the rat

Sergio Martínez-Bellver[1] (iD), Ana Cervera-Ferri[1], Aina Luque-García[1], Joana Martínez-Ricós[1], Alfonso Valverde-Navarro[1], Manuel Bataller[2], Juan Guerrero[2] and Vicent Teruel-Marti[1]

[1]*Neuronal Circuits Laboratory, Department of Anatomy and Human Embryology, University of Valencia, Valencia, Spain*
[2]*Digital Signal Processing Group, Department of Electronics and Engineering, University of Valencia, Burjassot (Valencia), Spain*

Key points

- The nucleus incertus is a key node of the brainstem circuitry involved in hippocampal theta rhythmicity.
- Synchronisation exists between the nucleus incertus and hippocampal activities during theta periods.
- By the Granger causality analysis, we demonstrated a directional information flow between theta rhythmical neurons in the nucleus incertus and the hippocampus in theta-on states.
- The electrical stimulation of the nucleus incertus is also able to evoke a phase reset of the hippocampal theta wave.
- Our data suggest that the nucleus incertus is a key node of theta generation and the modulation network.

Abstract   In recent years, a body of evidence has shown that the nucleus incertus (NI), in the dorsal tegmental pons, is a key node of the brainstem circuitry involved in hippocampal theta rhythmicity. Ascending reticular brainstem system activation evokes hippocampal theta rhythm with coupled neuronal activity in the NI. In a recent paper, we showed three populations of neurons in the NI with differential firing during hippocampal theta activation. The objective of this work was to better evaluate the causal relationship between the activity of NI neurons and the hippocampus during theta activation in order to further understand the role of the NI in the theta network. A Granger causality analysis was run to determine whether hippocampal theta activity with sensory-evoked theta depends on the neuronal activity of the NI, or vice versa. The analysis showed causal interdependence between the NI and the hippocampus during theta activity, whose directional flow depended on the different neuronal assemblies of the NI. Whereas type I and II NI neurons mainly acted as receptors of hippocampal information, type III neuronal activity was the predominant source of flow between the NI and the hippocampus in theta states. We further determined that the electrical activation of the NI was able to reset hippocampal waves with enhanced theta-band power, depending on the septal area. Collectively, these data suggest that hippocampal theta oscillations after sensory activation show dependence on NI neuron activity, which could play a key role in establishing optimal conditions for memory encoding.

Introduction

Synchronisation of oscillatory activity in distributed neuronal networks reflects the dynamic interactions that underlie information coding (Singer, 1999; Buzsáki, 2002; Foster & Wilson, 2006; O'Neill *et al.* 2008). In the hippocampus, the 'active' state is reflected by highly rhythmic oscillations of the local field potential at theta frequencies (4–10 Hz) (Buzsáki, 2002; Grastyán *et al.* 1959; Green & Arduni, 1954; Jouvet, 1969; Vanderwolf, 1969). These oscillations have been extensively described as being related to sensorimotor integration, spatial navigation and memory (Bland, 1986; O'Keefe & Recce, 1993; Huerta & Lisman, 1995; Bland & Oddie, 1998; Buzsáki, 2002, 2005).

Hippocampal theta rhythmicity is largely driven by subcortical distributed neuronal assemblies, which are involved in the generation, maintenance and modulation of the theta state (Faris & Sainsbury, 1990; Kirk & McNaughton, 1991; Alonso *et al.* 1996; Kirk *et al.* 1996; Kocsis & Vertes, 1996; Young & McNaughton, 2009). A complex network, which includes the septal area, posterior hypothalamus, mammillary area and mesopontine nodes, among others, exhibits oscillatory field activity coupled to hippocampal theta waves (Mitchell & Ranck 1980; Alonso & García-Austt, 1987*a,b*; Kirk & McNaughton 1991; Alonso *et al.* 1996; Kirk *et al.* 1996; Kocsis & Vertes 1996; Bassant & Poindessous-Jazat 2001). However, as the mechanisms involved in the coordination of distributed theta activities remain unclear, it is worth studying their dynamics to gain a better understanding of extrahippocampal theta coding.

A large body of evidence has shown the functional relationship between the brainstem and hippocampal theta rhythm (Pignatelli *et al.* 2012, for a review). The pontine nucleus incertus (NI), which belongs to the ascending brainstem–diencephalo–septal systems, is closely interconnected to the key nodes of the theta network (Goto *et al.* 2001; Olucha-Bordonau *et al.* 2003). NI neurons connect the reticular pontine oralis nucleus (RPO), usually identified as the main activator of oscillation, with the medial septum–diagonal band of the Broca complex (MS/DBv), considered to be the pacemaker of rhythm (Teruel-Martí *et al.* 2008). Studies by our group have focused on analysing the interdependence of the NI and the hippocampus through theta waves. NI activation induces theta rhythmicity in the CA1 area of the hippocampus. Sustained hippocampal theta activity, elicited either by RPO stimulation or by sensory activation, leads to a differential activity of NI neurons. Moreover, NI inactivation or lesion blocks the RPO (Nuñez *et al.* 2006). During hippocampal theta periods, the NI local field potential presents a synchronised oscillatory theta pattern (Cervera-Ferri *et al.* 2011) and, more specifically, a subpopulation of NI neurons shows theta firing coupled to hippocampal theta waves (Martínez-Bellver *et al.* 2015).

Studies by other groups have evidenced a proportion of NI neurons whose firing is coupled to the hippocampal theta after the local infusion of corticotropin-releasing hormone (CRH) in the NI itself (Ma *et al.* 2013). By taking into account the connections of the NI (Goto *et al.* 2001; Olucha-Bordonau *et al.* 2003), the immunoreactivity for CRH receptors (Potter *et al.* 1992, 1994; Chalmers *et al.* 1995) and the activation of NI neurons by stress (Bittencourt & Sawchenko, 2000; Banerjee *et al.* 2010), it has been proposed that NI neurons could be stress- and arousal-responsive, and involved in the integration of emotional and cognitive processes.

In the first part of the present work, we sought to analyse the temporal and directional dynamics of the synchronisation between the NI and the hippocampus. We tested the hypothesis that the coherent activities between both areas would show a temporal and preferential causal relationship, with defined directionality during theta periods. In order to delineate the patterns of interaction between both oscillators during experimental theta activation, time–frequency and causality methods were applied. The Granger causality analysis is an efficient method for assessing the effective coupling direction of the signals sourced from a set of interconnected nodes (Granger, 1969; Ding *et al.* 2006; Seth, 2007). Here we applied Granger's notion to identify the net directionality of the bidirectional communication between the local field potential of the hippocampus and the single-unit activity of the NI. The analyses focused on determining whether there was any causal – meaning directional – influence between them.

Our study also aimed to clarify some functional aspects of the role of the NI during brainstem-induced theta activation. In this sense, one viable mechanism by which hippocampal theta rhythmicity may elicit mnemonic processing is by resetting the theta wave, in which ongoing theta becomes phase-locked to incoming sensory stimuli (Adey, 1967; Givens, 1996; Brankack *et al.* 1996; Vinogradova *et al.* 1996).

Methods

In this study, three groups of results are included. The first group is a reanalysis of a subset of data which appeared in a previously published study that focused on the single-unit characterisation of NI neurons coupled to hippocampal theta rhythmicity (Martínez-Bellver *et al.* 2015). This group included 56 cases of well-isolated single units in conjunction with simultaneously recorded local field potential (LFP) signals. Full details about the experimental set-up can be obtained from the original study. Here we provide only the essentials.

A control group ($n = 8$) was added to study the dependency of the NI on the sensory activation of the hippocampal system. In a third experimental group

($n = 16$), we assessed the hypothesis of the NI as a driver of the phase resetting of hippocampal theta oscillations.

Ethical approval

The present work complies with the ethical principles under which *The Journal of Physiology* operates. All the experimental procedures were reviewed by the Research Ethics and Animal Welfare Committee of the University of Valencia (UV) in accordance with European Communities Council Directive (2010/63/EU) on the protection of animals used for scientific purposes. Adult female Sprague–Dawley rats (250–300 g) were used in the present study. Animals were supplied by Janvier (Le Genest St Isle, France) and maintained until the day before the experiment in the animal facilities at the Faculty of Medicine (UV). Experiments were designed to minimise the number of animals used and their suffering. Animals were housed under controlled temperature conditions ($23 \pm 3°C$) in a regular light–dark cycle, with food and water provided *ad libitum*.

Surgery methods

Rats were urethane-anaesthetised (1.5 g kg^{-1} I.P.), with supplemental doses of anaesthetic when the amplitude of the slow waves (< 2.5 Hz) in the hippocampal field potential decreased during non-stimulated periods. Lidocaine 2%/epinephrin (S.C.) was added as a local anaesthetic to block the nerves of the scalp and pressure points: zygomatic (0.05 ml) and ophthalmic (0.1 ml) nerves and C2 fibres (0.2 ml). Surgery started only when plantar and tail pinch reflexes disappeared. Animals were then secured to a stereotaxic frame and maintained at 37–38°C with a heating pad. Following a midline sagittal incision, trephine holes were drilled above the dorsal hippocampus in the CA1 area (AP: –3.5 mm, L: 2.5 mm and DV: 2.5 mm) and the NI (AP: –9.7 mm, L: 0.0 mm and DV: 6.4 mm), referenced from bregma, and according to the atlas of Paxinos & Watson (2004). Due to interindividual variability and the small size of the NI, proportional corrections were made with reference measures (9 mm from bregma to interaural), as previously described (Teruel-Martí *et al.* 2008), in order to enhance precision. For the inactivation experiments of the septal region, an additional trephine hole was drilled above the medial septum (AP: 0.7 mm, L: 0.0 mm and DV: 6.2–7.5 mm).

Electrophysiological methods

Recording protocols. The methods used to acquire electrophysiological recordings have been previously described in detail (Martínez-Bellver *et al.* 2015). Briefly, the hippocampal LFP was recorded with a steel Teflon-coated monopolar macroelectrode (120 μm diameter; World Precision Instruments, Aston, Stevenage, UK), placed at the CA1 region of the hippocampus and referenced against an indifferent electrode placed in the cerebellar epidural space. The final position was determined by maximising the amplitude of the LFP in response to a mild tail pinch application.

Raw field activity was recorded with a first differential AC pre-amplifier (Grass p55; ×10, Grass Technologies, West Warwick, RI, USA) complemented with a second amplification (Cibertec amplifier, ×100; model: AMPLI4G21, Cibertec, Madrid, Spain) and filtered online (0.3–30 Hz). Data were collected on a personal computer via a Cambridge Electronic Design (Cambridge, UK) 1401 interface using the Spike2 software (Cambridge Electronic Design; sampling rate, 1000 Hz).

Single unit activity was recorded in the NI concurrently with the hippocampal LFP. Borosilicate glass micro-electrodes, filled with 3 M saline, were used with *in vitro* impedances of > 5.0 MΩ. The capillary was placed on the NI coordinates and was lowered using a one-axis motorised stereotaxic micromanipulator (Narishige, Japan). Single-cell activity was amplified (DAM 80; World Precision Instruments, Sarasota, FL, USA) and monitored on a digital oscilloscope with an audio monitor as a complement. Only the single-unit signals that showed a stable waveform and a high signal-to-noise ratio (4:1 or more) were selected. Single-unit recordings were sampled at 20 kHz and bandpass-filtered at 250–5000 Hz.

Stimulation procedures and functional inhibition. *Sensory stimulation and NI blockade.* After a hippocampal spontaneous activity period (30 s), tail pinch was applied (30 s) by means of a clamp with regulated closure to warrant a similar stimulation level across experiments. For the purpose of verifying whether the NI is a key node in sensory processing, in some cases ($n = 8$) we performed a temporary inhibition of the NI by pharmacological blockade following tail pinch. Inhibition was carried out in the NI area by injecting 1 μl of the GABA$_A$ agonist muscimol (75 ng, 0.5 μl), delivered at 0.5 μl min^{-1} with a Hamilton syringe.

Electrical stimulation. Electrical stimulation of the NI ($n = 16$) was applied by means of bipolar electrodes (two twisted 120 μm-diameter bluntly cut stainless steel wires). Prior to each experiment, the optimal depth of the stimulation electrode was determined by sequentially applying short trains at a given intensity and measuring the evoked theta increase in the hippocampal LFP. When the spontaneous hippocampal activity returned to basal values, the definitive stimulation was applied (0.1 Hz electrical pulses at 100–500 μA, 0.2 ms).

The involvement of the septal area in the NI activation effect was assessed by the transient inhibition of the medial septum (5 of the 16 animals). The blockade was made

by injecting 0.7–1 μl of 5% procaine with a Hamilton syringe (0.1 μl min^{-1}), delivered along the dorsoventral coordinates of the septal area.

Terminal procedures

At the end of the experimental procedures, animals were killed under terminal anaesthesia. Animals were deeply anaesthetised with sodium pentobarbital (100 mg kg^{-1} 20%; Dolethal Vetoquinol, Madrid, Spain) and perfused with 0.1% heparinised saline (0.9%, pH 7) and 4% paraformaldehyde (Sigma-Aldrich, St Louis, MO, USA) for histological verification of electrode tracks.

Histological verification

Final electrode positions were verified histologically by identifying the track lesion. Coronal sections (40 μm) were obtained by freezing microtomy. The placement of electrodes was verified by the Giemsa method, as shown in Fig. 1.

Data analysis

Digitised spike trains were imported into the offline spike-sorting module of the Spike2 software. Spike-sorting methods were applied by a principal component analysis and a supervised k-means clustering algorithm. Isolated spike units with interspike intervals < 2 ms, compatible with the refractory period, were removed from the analysis.

Raw signals were then imported to the Matlab development environment (The MathWorks, Natick, MA, USA) for offline analyses, which were performed using built-in self-developed routines. The theta band was defined within the 3–8 Hz range by taking into account the downward shift of the theta frequency range under urethane anaesthesia (Leung, 1985).

In order to correlate both neuronal and LFP signals in the same domain, single-unit events were binarised (i.e. converted into a 0–1 series with 1 at the localisation of spikes, and 0 elsewhere) and converted into a spike density

function (SDF; Fig. 2*C*). Briefly, using a continuous and symmetric function (kernel), the firing frequency can be achieved as a smooth and continuous function in the time domain by convoluting the kernel at each spike occurrence time. We used a Blackman–Harris kernel of 1000–5000 sampled points as an appropriate width (Szucs, 1998). Both the hippocampal LFP and the spike density of the NI signal were then down-sampled at 200 Hz and the *Z*-score was normalised.

Wavelet analysis. Signals were processed in the time–frequency domain by the continuous wavelet transform, as described by Torrence & Compo (1998). Wavelets were extensively applied to analyse the neural signals. Briefly, each time series was convoluted with the complex Morlet wavelet, defined as:

$$\psi_0(\eta) = \pi^{-1/4}\exp(i\omega_0\eta)\exp(-\eta^2/2)$$

where central frequency was $\omega_0 = 6$, whose value is chosen to optimise the time–frequency resolution. This transform is well suited to describe phasic or transient events by multiscale decomposition in the time and frequency domains. The wavelet transform output at each time, $W(s)$, leads to the power ($|W(s)|^2$) and phase ($\tan^{-1}\text{Re}\{W(s)\}/\text{Im}\{W(s)\}$) (being Re the real part and Im the imaginary part) of the signal on each scale s (frequency). Power values were normalised to scale, $s^{-1}|W(s)|^2$, to avoid scale-dependent biased values (Liu *et al.* 2007). The time-averaged wavelet spectrum over a certain period was calculated as:

$$\bar{W}^2(s) = \frac{1}{N}\sum_{n=1}^{N}|W_n(s)|^2$$

a measure of the power spectra derived from the time–frequency wavelet spectrogram.

Mutual information. Shared information that derives from the mutual information (MI) concept reflects the degree of interdependence between two time series. MI is able to identify non-linear relations among neural signals,
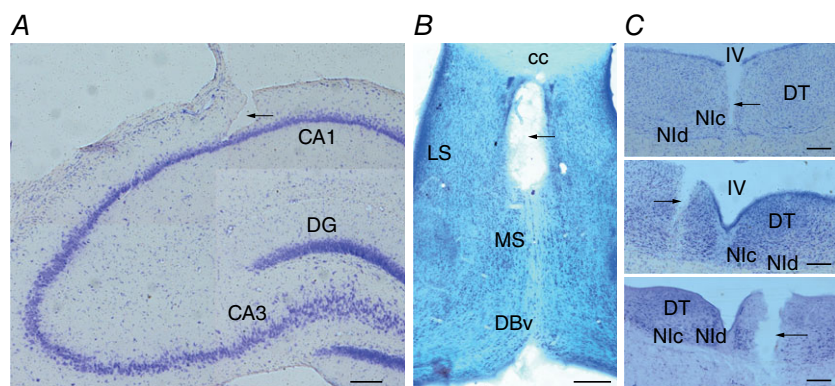
Figure 1. Histological verification of the electrode placement
A, lesion of the LFP recording electrode aimed at the hippocampal CA1 (composite image). *B*, injection site lesion in the MS (composite image). *C*, top, trace of the muscimol injection in the NI. Middle, electrical stimulation electrode misplacement in a neighbouring area to the NI. Bottom, electrical stimulation electrode lesion inside the boundaries of the NI. [Colour figure can be viewed at wileyonlinelibrary.com]

which are underestimated by linear methods (Freiwald *et al.* 1999). A subset of the wavelet power matrices was extracted for frequencies between 3 and 8 Hz for the NI and hippocampal signals. From the wavelet power distribution, we applied the Shannon entropy concept,

defined from the Information Theory (Shannon, 1948) as:

$$H(X) = -\sum_{i=1}^{N_x} p_x(i) \cdot \log_2 p_x(i)$$
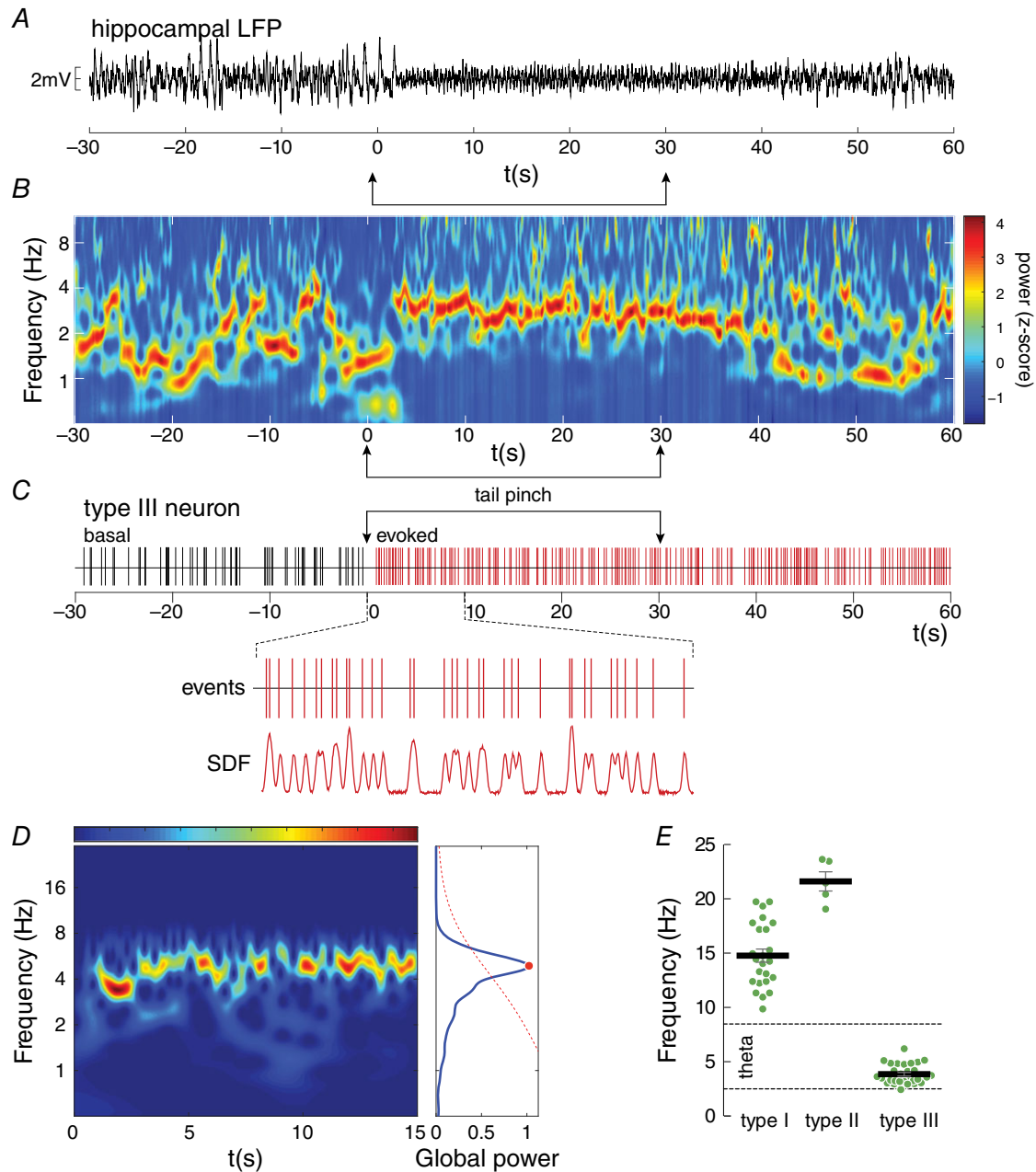
Figure 2. Effect of the tail pinch on hippocampal waves and the firing changes of the NI
A–C, a representative case of a tail pinch trial is shown as the raw signal of the hippocampal LFP (*A*), its spectral distribution was visualised by a wavelet spectrogram (*B*), and the simultaneous firing pattern of a representative NI neuron (*C*). The time–frequency decomposition in *B* is shown with colour-coded values (high power with a warm colour), which indicates wavelet power coefficients (Z-scored). *D*, wavelet determination of the significant power peaks of the NI neuronal activity. *E*, distribution of the firing frequencies, for the three functional types of NI neurons, during hippocampal theta presence. The nomenclature follows that previously described in Martínez-Bellver *et al.* (2015). [Colour figure can be viewed at wileyonlinelibrary.com]

where $p_x(i)$ represents the relative frequency of the ith bin ($\sum_i p_x(i) = 1$). The Shannon entropy of the joint distribution is given by:

$$H(X, Y) = -\sum_{i=1}^{N_x} \sum_{j=1}^{N_y} p_{xy}(i, j) \cdot \log_2 p_{xy}(i, j)$$

Then MI was calculated as:

$$\text{MI}(X, Y) = H(X) + H(Y) - H(X, Y)$$

where X and Y are the power distributions of both signals.

Causality analysis. Granger causality (Granger, 1969) is the most widely established means to identify causal relations between two times series. Given two time series, X and Y, to assess whether X causally influences Y, Y is first modelled as a univariate autoregressive series with the error correction term ξ:

$$Y_i = \sum_{j=1}^{p} a_j Y_{i-j} + \xi$$

where p is the order of the model and a_j the coefficients of regression. Then, Y is remodelled using the X series as causal side information, where ξ_R is the new residual value:

$$Y_i = \sum_{j=1}^{p} [b_j Y_{i-j} + c_j X_{i-j}] + \xi_R$$

Provided that the signals show covariance stationarity, Granger causality is defined as a logarithmic scaled ratio between the variances of the residuals:

$$G_{X \to Y} = \log \frac{\text{var}(\xi)}{\text{var}(\xi_R)}$$

Thus $G_{X \to Y}$ and $G_{Y \to X}$ represent the causal values for each directional flow.

In our work, the causality analysis in the time and frequency domains was performed by means of the functions implemented in the GCCA (Seth, 2010) and HERMES (Niso *et al.* 2013) libraries. First of all, with the Z-scored signals, covariance stationarity was verified by the augmented Dickey–Fuller test (ADF) and the Kwiatkowski, Phillips, Schmidt and Shin test (KPSS). The model order was estimated *a priori* by the Akaike information criterion. The significant interactions of the time domain causality were assessed according to the null hypothesis that coefficients a_j were zero, as established by the F test with Bonferroni correction.

In the frequency domain, the directed transfer function (DTF; Kamiński & Blinowska, 1991) is related to Granger causality. The main difference lies in the fact that the DTF transforms the autoregressive model into the spectral domain (Kamiński *et al.* 2001). In order to estimate the significance of the causal peaks in the frequency domain, surrogate signals were generated from the original data. The phases of each signal in the frequency domain were randomised. Finally, the modified signal was transformed back into the time domain. Phase randomisation destroyed the structure in the input signal. For each epoch, 200 surrogate data were constructed and the spectral causal distribution was compared with the original signal.

Theta resetting analysis. Raw LFP data from 500 ms pre-stimulus to 750 ms post-stimulus were averaged over 200 trials and time-locked to the onset of the stimulus in order to compute the average evoked potential. The resultant amplitude and latency of the averaged waveform were analysed and subjected to a wavelet analysis to quantify the resetting phenomena. The dominant frequency at the theta band was determined through the wavelet spectrogram, and then trials were filtered at this frequency ± 2 Hz (Butterworth bandstop filter). The average evoked potential was recomputed as the representative wave of electrical stimulation.

Phase resetting was considered when the phases of the signal showed a uniform distribution over trials. From the comparisons, the instantaneous phase was extracted from the wavelet coefficients. Rayleigh's test for phase uniformity at a given time was used to test whether the signals presented a uniform distribution (null hypothesis) or a significant phase alignment ($P < 0.05$). The time course of the P-values was then represented. The time when the P-value showed significant phase locking ($P < 0.05$), if the theta wave was maintained for at least one full cycle, was taken as the beginning of the phase reset.

Statistical methods

Statistical comparisons were made by parametric or non-parametric tests, wherever appropriate, after checking the assumptions of normality (Shapiro–Wilks test; $P < 0.05$ to reject) and homoscedasticity (Levene's test; $P < 0.05$ to reject). For the paired comparisons, Student's t test as a parametric test, and Wilcoxon's matched-pairs signed-ranks test as a non-parametric test were performed. The Kruskal–Wallis or Friedman's test was used as a non-parametric test for the comparisons made between unpaired or paired samples, respectively. The threshold for significance between the comparisons was accepted at the 95% ($P < 0.05$) or 99% level ($P < 0.01$, as a double significant value). All the results were expressed as the mean $\pm$ standard error of the mean (SEM). These calculations were made using the R statistical package (http://www.r-project.org/).

Results

The correct aim of the electrode at the hippocampal CA1 layer was checked in all the animals (Fig. 1*A*). The Giemsa staining showed that in the electrical stimulation experiment, the stimulation electrode was placed inside the boundaries of the NI in 11 of the 16 animals (Fig. 1*C*, bottom), of which five were used for the septal inactivation procedure (Fig. 1*B*). The animals with a misplaced stimulation electrode (5 of 11; Fig. 1*C*, middle), were used as an electrical stimulation control group. Finally, for the NI inactivation experiment, muscimol injections inside the boundaries of the NI were correctly achived in 5 of the 8 rats (Fig. 1*C*, top).

Tail pinch activation was used to characterise the single-unit activity of the NI at sustained hippocampal theta rhythmicity (Fig. 2). Under urethane conditions, the hippocampus showed spontaneous theta rhythmicity (3–8 Hz) alternating with irregular delta waves, whose proportion depended on both the depth of anaesthesia and environmental stimuli. Sensory activation by tail pinch (stimulus epoch, 30 s) evoked sustained theta oscillations in the hippocampal CA1 region (Fig. 2*A* and *B*). Fifty-six neurons that belonged to the tegmental NI, and correlated with theta activity, were isolated for this study. The exclusion criteria were: no hippocampal response to stimuli, no changes in the firing rate of the NI single units or the histological verification of misplaced electrodes.

NI neurons showed theta activity that correlates with hippocampal rhythmicity

As previously mentioned, the hippocampal LFP cycled mostly between delta waves (< 2.5 Hz), with short epochs of spontaneous theta (Fig. 2*B*). After tail pinch, the LFP shifted predominantly to the theta range (3–8 Hz). Although the tail pinch effect was observed, this oscillatory profile was mostly maintained over time. The wave content was controlled to give at least 25% of theta activity in the time domain after sensory stimulation.

NI neurons ($n = 56$) were classified following the criteria used in Martínez-Bellver *et al.* (2015). Given the conversion from single-unit events into the SDF, we characterised the oscillatory pattern of the SDF in the 15 s window after tail pinch. In the time–frequency domain, we determined the frequencies of the power peaks with significant values by means of the time-averaged wavelet spectrum (Fig. 2*D*). These measures were then compared with the firing rates described in Martínez-Bellver *et al.* (2015). Neuron types I, II and III were identified on the basis of their response to sensory stimulation. Type I neurons ($n = 24$; Fig. 2*E*, left) showed peaks of frequency within the 10–20 Hz range (14.47 ± 0.60 Hz), which were clearly comparable to the previously described firing

rate (one-sample *t* test; theoretical mean: 14.10 spikes s^{-1}; $t = 1.102$; $P = 0.28$). Type II neurons ($n = 6$; Fig. 2*E*, middle), with a minor isolated population given their low proportion, obtained the highest frequency values during the sensory evoked epochs (21.61 ± 0.88 Hz; one-sample *t* test; theoretical mean: 20.48 spikes s^{-1}; $t = 1.28$; $P = 0.27$). The population of type III neurons ($n = 26$; Fig. 2*E*, right) displayed wavelet activities in the theta-range frequencies (3.85 ± 0.17 Hz), which were slightly lower than the firing rate (one-sample *t* test; theoretical mean: 5.3 spikes s^{-1}; $t = 8.6$; $P < 0.01$).

Overall, these data ensured the criteria to categorise NI neurons were met according to our previous work, with oscillatory profiles that matched the original classification.

Hippocampal theta evoked by tail pinch depends on NI activity

One question we firstly considered was the dependency of the NI on sensory-induced theta field activity. We assessed the effect of the inactivation of the NI on hippocampal theta rhythmicity with tail pinch ($n = 5$). According to the well-established effect of tail pinch in rodents, the hippocampus increases the relative power of the theta band compared with a spontaneous basal period (Fig. 3*A*).

Our results indicated that the tail pinch-evoked theta somehow depended on NI activity since its neurochemical inactivation prevented the sensory effect (Friedman's test, $\chi^2 = 7.6$; $P < 0.05$; Fig. 3*A*, left). The multiple comparisons (Dunn's correction) among all three conditions gave significant differences between basal spontaneous theta power (0.10 ± 0.01) and the tail pinch-evoked theta (0.30 ± 0.02; $P < 0.05$). Conversely following NI inactivation by muscimol microinfusion, the hippocampal theta power was similar to that during the basal period (0.11 ± 0.007). The theta propensity measure, defined as the time in theta frequencies normalised to the full epoch with the theta relative power above the third quartile, obtained similar outcomes (Friedman's test, $\chi^2 = 7.6$; $P < 0.05$; Dunn's correction for multiple comparisons; Fig. 3*A*, right). The hippocampal theta propensity during the basal period (0.17 ± 0.02) was clearly lower than after tail pinch activation (0.68 ± 0.04; $P < 0.05$). Once again with NI inactivation, values were similar to the basal levels (0.16 ± 0.02; $P > 0.05$).

NI neurons and hippocampal theta rhythm showed causal relations

Previous work by our group has evidenced correlated theta activity between NI neurons and hippocampal theta oscillations (Nuñez *et al.* 2006; Martínez-Bellver *et al.* 2015). However, the directionality of this coupling is unclear. Thus in part, the aim of the present report

is to provide information about the causal interactions between NI neurons and hippocampal theta rhythmicity. The Information Theory aims to describe the local dynamics in space and time of the information transfer. In these terms, MI quantifies the information shared by two random variables within a probabilistic framework. As detailed in Methods, we examined the degree of interdependence between NI neuronal activity and tail pinch-evoked hippocampal theta. For the statistical analysis, we performed both lots of MI to confirm the interrelation and causality analyses in order to assess directionality.

Mutual information. On the one hand, MI was calculated from the power distributions of the NI and hippocampal signals extracted from the wavelet spectra. From the trials, we extracted four time segments of 10 s (one pre-stimulus segment and three consecutive post-stimulus segments). Following stimulation, MI values increased significantly (Friedman's test; $\chi^2 = 23.30$, $P < 0.01$; Fig. 3*B*) and progressively recovered similar values to the basal ones. During the pre-stimulus epoch, MI was 0.11 ± 0.0071 bits and increased significantly in the first (0.17 ± 0.0097 bits; Dunn's test, $P < 0.001$) and the second (0.15 ± 0.0123 bits; Dunn's test, $P < 0.01$) post-stimulus interval, respectively. During the last post-stimulus epoch analysed, MI had returned to the basal values (0.13 ± 0.0091 bits; Dunn's test, $P > 0.9$). This approach conferred consistency to the existence of an interrelation between both neural populations.

Granger causality. We next quantified the Granger causal relationship between spike activity and the hippocampal

signal in the frequency domain. The causality analysis was conducted on a time series that reflected activity within the two source-localised brain areas: the hippocampal LFP and the SDF obtained from single-unit NI activity. Samples exhibited non-stationary features. Therefore, the time series were divided into short overlapping (50%) segments (5 s). We chose this segment length to strike a balance between stationarity and model fit. Whereas shorter time series were more likely to be stationary, longer samples allowed better parameter estimations for the linear autoregressive models. As a first approach, the spectral DTF distribution allowed the isolation of precise differences in the causal relation between both signals. With this analysis, the causal flow at a given frequency is represented by salient peaks in one direction, with clearly non-significant lower values in the opposite direction; i.e. a net directionality between signals, in contraposition to a non-directional flat scenario.

Significant causal interactions were detected between NI spike activity and the concurrent signals recorded from the hippocampus (Fig. 4). All three neuronal types presented activities with a predominant asymmetric relation with hippocampal waves, but differences were detected between neuronal subtypes. Type III neurons were the population that revealed more consistent causal activity in the unit-to-LFP direction on the theta band. Figure 4*A* illustrates representative trials with the causal distribution for each direction for a type III neuron. Most basal non-theta epochs did not show a net flow between signals, with under-threshold DTF values in both directions (Fig. 4*A*, first figure). Segments with predominant theta rhythmicity were detected both during spontaneous periods (Fig. 4*A*, second figure) and following tail
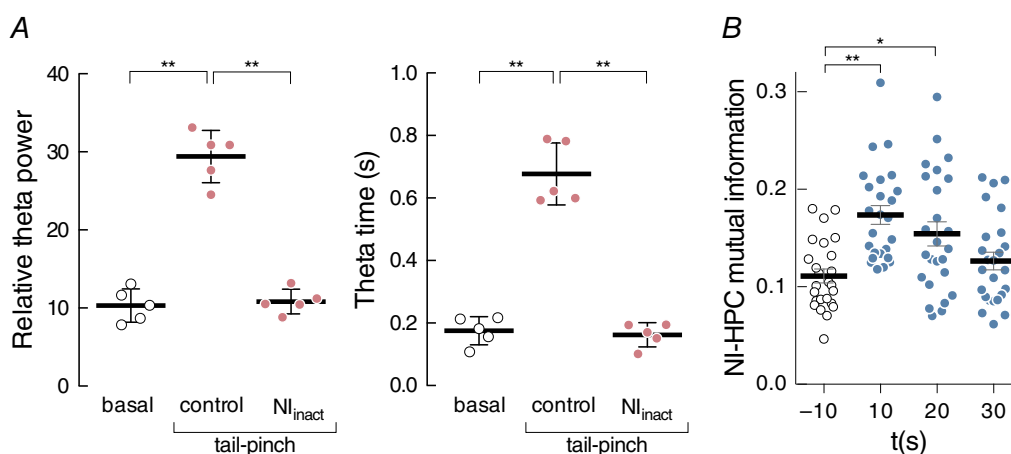
Figure 3. Evoked theta response in the hippocampus and mutual information analysis, related to the NI
A, the effect of the relative theta power in the hippocampus (HPC) during basal conditions and during sensory evoked theta power both in control conditions and with the NI inactivation. The right figure shows the relative time that the HPC remains in theta during the evoked period (relative to 30 s). *B*, mutual information representation, between the NI and hippocampus, during basal conditions (−10 s, white dots) and during evoked theta activity (10, 20 and 30 s, blue dots). [Colour figure can be viewed at wileyonlinelibrary.com]
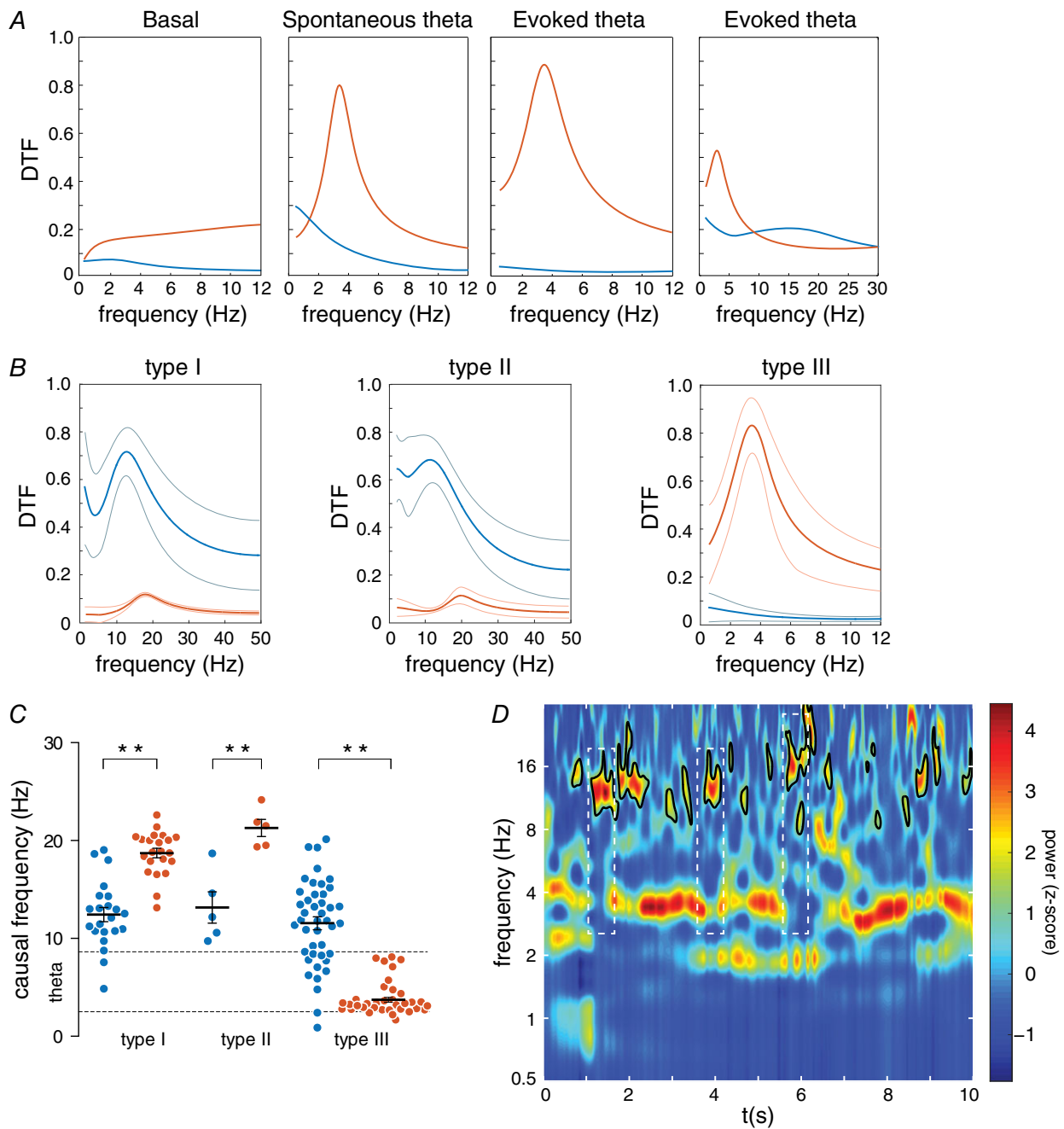
Figure 4. Bivariate causal analysis performed with the hippocampal LFP and the spectral density function (SDF) extracted from NI neurons

A, spectral distribution of the directed transfer function (DTF) for both directionalities (blue for HPC→NI; orange for NI→HPC) in an example of the type III neuron. Note the presence of predominant DTF peaks in the spontaneous and evoked state, which represent frequency with significant causal values, which are clearly different from values for reversal directionality. *B*, average DTF distribution for the three neuronal types. Thick lines represent the average values and thin lines indicate standard deviation. *C*, causal frequency distribution calculated as peaks in DTF spectra. The mean values and standard error of the mean are represented for each neuronal type (blue for HPC→NI; orange for NI→HPC). *P < 0.05 and **P < 0.01. *D*, wavelet spectrogram of the hippocampal signal for a representative epoch to visualise presence of beta activity in accordance with the theta peaks detected in the DTF spectra for the type I neurons. White dashed line boxes highlight beta epochs isolated in non-theta periods. [Colour figure can be viewed at wileyonlinelibrary.com]

pinch (Fig. 4*A*, third figure). In both cases, the DTF values showed over-threshold peaks on the theta band (permutation test, $P < 0.01$), in which NI→hippocampus (HPC) directionality was significant (DTF ~0.8; $P < 0.01$), unlike the reverse one (DTF < 0.2; $P > 0.05$). Furthermore, evoked epochs also showed causal beta peaks in the HPC→NI directionality (Fig. 4*A*, fourth graph).

These profiles were conserved in the average spectral distribution of all the epochs with significant causal peaks (Fig. 4*B*). The group data for type III neurons revealed that the theta range (3.74 ± 0.25 Hz) was the significant causal frequency in the NI→HPC interaction (Fig. 4*B*, right). Even so, this group also presented isolated significant DTF peaks in non-theta episodes, but within the 10–20 Hz band range, unpreserved in the average representation (Fig. 5*A*). Hence, this demonstrates a bidirectional flow between both areas with a different oscillatory pattern per direction.

Type I (Fig. 4*B*, left) and II (Fig. 4*B*, middle) neurons mostly showed high over-threshold DTF values with the LFP-to-unit directionality within the 10–20 Hz range. These neuronal typologies had significant causal peaks at 12.43 ± 0.72 and 13.16 ± 1.61 Hz for HPC→NI directionality, respectively. The opposite flow also had lower but significant peaks within different ranges of frequencies: type I, 18.72 ± 0.48 Hz ($t = 4.42$, $P < 0.01$); and type II, 21.29 ± 0.88 Hz ($t = 7.47$, $P < 0.001$).

However, no peaks within the theta range were found in the spike-to-LFP direction for any of these neuronal subtypes under evoked conditions.

Hence, we reveal here that a different directionality governs the flow of information between the NI and the hippocampus in the theta activity context. The causal interaction HPC→NI was generally manifested within the 10–20 Hz band range, without significant differences in the frequency range between the three neuronal subtypes (Kruskal–Wallis, $H = 0.42$, $P = 0.81$). The NI→HPC flow was present with different firing profiles depending on neuronal type (Kruskal–Wallis, $H = 49.70$, $P < 0.001$) and with consistent spike-to-LFP directionality only for type III neurons.

Exploiting the temporal pattern of the causal peaks detected for both causal directions complemented this first description. We used the normalised difference of the two causality quantities as a measure of the causal relationship between the two directional variants. Figure 5*A* illustrates the causal flows in the time-frequency domain for a representative trial of type III neurons. On this causal map, with a colour code, we clearly observed the presence of warm regions, which indicated epochs with the NI→HPC directionality. As represented, these regions were limited to the theta range of frequencies. While some theta bouts were detected under spontaneous conditions, their presence clearly increased after tail pinch. Despite
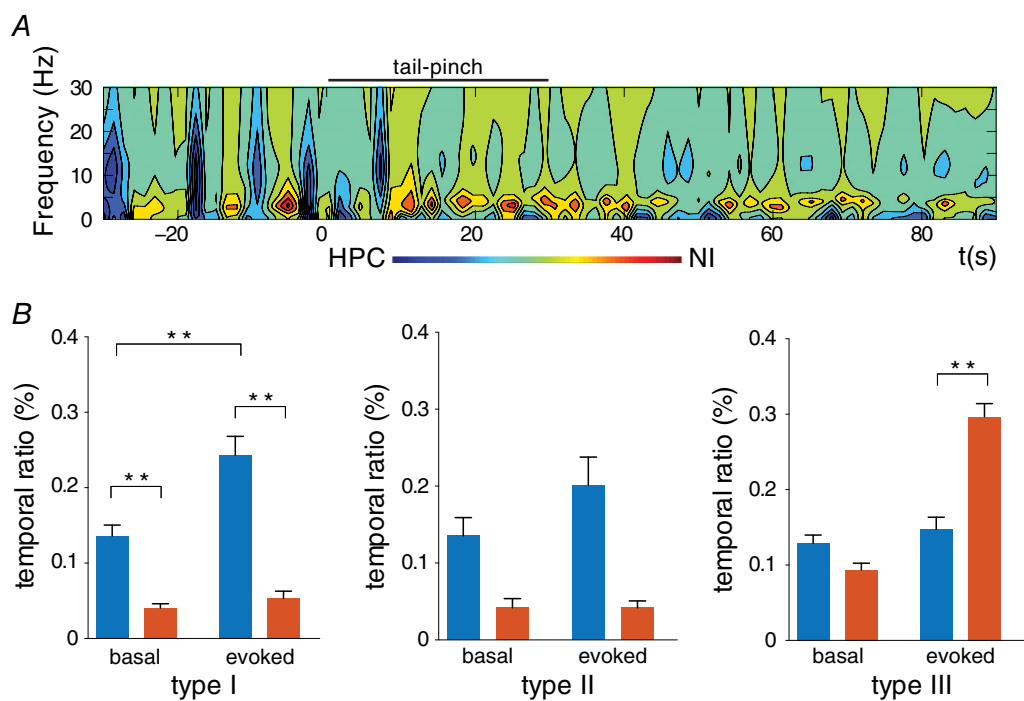
Figure 5. Causal relations between the hippocampal LFP activity and the NI neurons
A, time–frequency representation of the causal relation between the HPC and type III NI neurons; representative case. *B*, the temporal ratio statistics with the causal significance for each neuronal type, for both causal directions (blue for HPC→NI; orange for NI→HPC) and for each experimental state (basal and evoked states). *P < 0.05 and **P < 0.01. [Colour figure can be viewed at wileyonlinelibrary.com]

its weaker presence, the HPC→NI flow (cold regions) was also visualised, but on a different frequency band (10–20 Hz) and mainly during the pre-stimulus period.

In statistical terms, the three neuronal types distinctly exhibited different propensities for both causal directions (Fig. 5*B*). The times detected with a significant causal flow provided the temporal distribution of each direction. Type I and II neurons maintained a net causal flow from the hippocampus. Type I neurons (Fig. 5*B*, left) displayed mostly higher propensity in the HPC→NI direction under both conditions (basal: Wilcoxon's test, $W = -120$, $P < 0.001$; evoked, Wilcoxon's test, $W = -217$, $P < 0.001$), with a major temporal ratio in the same direction with tail pinch stimulation (Wilcoxon's test, $W = 260$, $P < 0.001$). In contrast, the presence of NI→HPC maintained lower values for both conditions (Wilcoxon's test, $W = 35$, $P = 0.09$). The type II neuron case (Fig. 5*B*, middle) was similar, despite the small number of cases that led to non-significant statistics, which could be considered only a tendency with a higher temporal ratio in the HPC→NI directionality (basal period: Wilcoxon's test, $W = -10$, $P = 0.12$; evoked period: Wilcoxon's test, $W = -15$, $P = 0.06$). Similarly, a slight change was observed between the basal and evoked periods in the reverse direction (Wilcoxon's test, $W = 10$, $P = 0.06$), which was once again taken as a tendency.

Conversely, type III neurons presented a distinguished NI→HPC propensity according to the hippocampal state (Fig. 5*B*, right). Whereas the temporal ratio for both directionalities gave comparable values during the basal epochs (Wilcoxon's test, $W = -215$, $P = 0.092$), weighty differences were recognised in the active state (Wilcoxon's test, $W = 654$, $P < 0.001$), along with a remarkable propensity to the NI→HPC flow. This dissimilarity was not observed when comparing the temporal ratios of the basal and evoked epochs for the HPC→NI direction (Wilcoxon's test, $W = 214$, $P = 0.08$).

In summary, it was possible to recognise both directionalities in the functional interaction of the NI and the hippocampus. Different patterns were distinguished across the neuronal populations of the NI: while type I and II neurons were predominantly receivers of descending hippocampal waves, type III neurons seemed to play an active role in hippocampal theta genesis after sensory stimulation.

NI electrical stimulation elicits theta wave readjustment in the hippocampus LFP

According to the aforementioned results, we first proved the essential role of the NI in hippocampal theta activation after tail pinch. Then we quantified the net directionalities in the interaction between the NI and the hippocampus under the ongoing theta. Finally, as our work aimed to clarify the mechanisms by which the NI could influence

the hippocampal theta, we noted from the causality analyses that a defined group of NI neurons showed theta spiking, which was generally able to anticipate hippocampal theta rhythmicity. Such evidence suggests an active role of NI neurons during hippocampal theta state periods. Therefore, what we analysed was the specific gating mechanism of the NI on hippocampal theta activity. Our hypothesis indicated that the NI could induce a phase resetting of theta oscillation as a mechanism. As will be discussed, this could allow the incoming inputs to the septohippocampal system to become temporally coupled under behaviourally relevant conditions.

Periodic electrical pulses (1 pulse per 5 s) were applied in the NI ($n = 11$) to elucidate the effect on hippocampal oscillations. Our findings revealed that even a single pulse in the NI sufficed to evoke a short epoch of theta waves of 2–3 cycles in the CA1. The signal filtered in the theta range showed amplitude peaks after the pulse (representative case in Fig. 6*A*, top). As shown, the spectral hippocampal LFP content exhibited a prominent post-stimulus theta bout (Fig. 6*A*, bottom). We observed a clear tendency of the trial-averaged epochs to exhibit oscillatory activity during the post-stimulus period compared with the pre-stimulus epoch (Fig. 6*B*). As a whole, the stimulus-evoked response implied increased hippocampal theta power ($Z = 2.93$; $P < 0.01$), which lasted 2.54 ± 0.16 theta cycles and with maximal value at 285.45 ± 34.55 ms. The presence of prominent cycles and a significant spectral peak at the theta frequencies in the post-stimulus average waveform suggested a possible phase reset of ongoing oscillatory activity rather than an additive evoked response. If no resetting occurred, the post-stimulus average waveform would result in a flat line.

Further evidence to support the theta phase reset came from comparing the distribution of phases across the trial epochs at each time point. A significance deviation from the uniform distribution of the post-stimulus period phases was tested by the Rayleigh test. Clear waveform readjustment following stimulation (Fig. 6*D*, top) indicated a higher degree of phase fixation upon theta onset (Rayleigh test, $P < 0.05$), and therefore a phase reset of theta waves after each pulse. This result suggested a hippocampal theta reset time-locked to the stimulus event. The time course representation of the *P*-values (Fig. 6*D*, bottom) indicated that the theta phases were fixed at 107.89 ± 33.57 ms after the stimulus, where phase uniformity lasted 406.55 ± 43.19 ms. The reset was observed at an average frequency of 5.59 ± 0.54 Hz and lasted 2.18 ± 0.23 cycles.

The electrode misplacement in the NI ($n = 5$) allowed us to perform a control analysis in order to assess whether the effect of the electrical stimulation was NI-specific. No theta power increase was observed after the electrical stimulation in the neighbouring areas to the NI ($Z = 0.54$; $P > 0.05$). In addition, the phase preference distribution

did not show a theta phase reset, with a uniform phase distribution in all cases (Rayleigh *P*-value > 0.05; Fig. 6*E*).

Inactivation of the medial septal area avoids NI-mediated hippocampal theta reset

The MS/DBv is one of the major projections of NI neurons (Goto *et al.* 2001, Olucha-Bordonau *et al.* 2003,

Teruel-Martí *et al.* 2008). The septal area was considered in order to determine the possible role of this structure in the hippocampal theta reset. For this purpose, MS/DBv was temporally inhibited with procaine infusion. After the microinjection, the same electrical stimulation protocol was applied to the NI. In all the analysed cases ($n = 5$), the mean theta band showed no significant increased theta power after stimuli following inactivation ($Z = -0.67$,
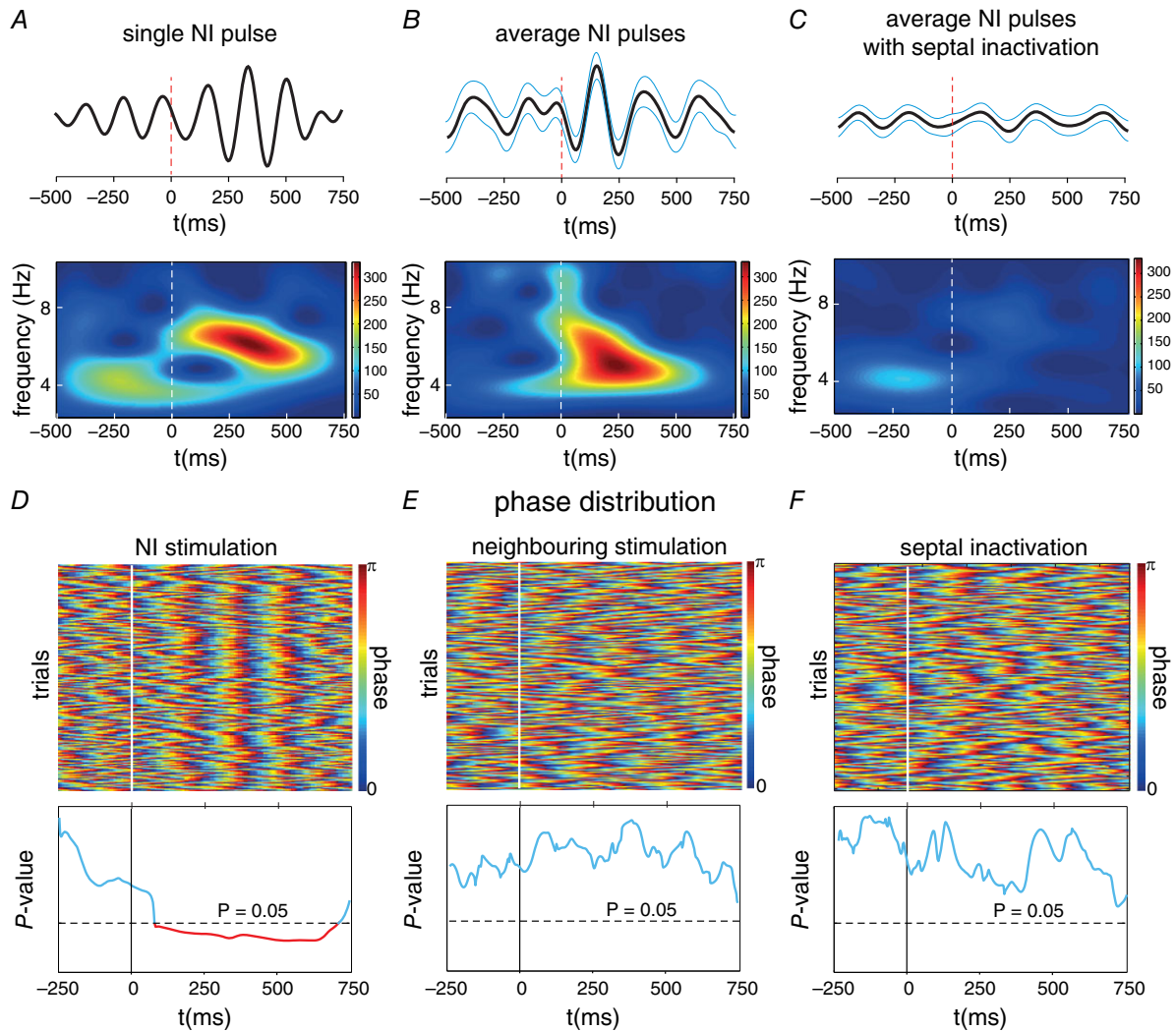
Figure 6. Phase-reset analysis of the hippocampal wave after electrical stimulation on the NI
A, wavelet spectrogram of a hippocampal LFP single trial (bottom) and the filtered signal within the theta range (top), with the theta increase shown after the electrical pulse. *B*, average filtered signal (top) and spectrogram (bottom) for all trials during an experimental session. As in a single pulse, a characteristic theta increase can be visualised as an effect of the electrical pulses in the NI. *C*, average filtered signal (top) and spectrogram (bottom) for all the trials during an experimental session after MS/DBv inactivation by muscimol infusion. Vertical dashed lines represent the electrical pulse in the NI and blue lines the SEM of the average signal. *D*, top, single-trial phase resetting evoked by the electrical pulses in the NI. Each horizontal line reflects the phase distribution of the theta-filtered hippocampal signal. Warm colours represent the phase peak at 180 deg. Bottom, Rayleigh's test of the phase distribution in the time domain for all trials during the same recording session. The horizontal dashed line is indicative of the threshold for statistical significance (*P* < 0.05). The values below the significance level (in red) were considered to define the phase-locking epoch between trials, and allowed the detection of the onset of reset. *E*, phase-trial representation (top) and Rayleigh's *P*-values (bottom) with the electrical stimulation in neighbouring areas of the NI. *F*, phase-trial representation (top) and Rayleigh's *P*-values (bottom) with the inactivation of the MS. [Colour figure can be viewed at wileyonlinelibrary.com]

$P > 0.05$). Figure 6*C* illustrates how no power change occurred in the hippocampal LFP within the theta range after applying electrical pulses. As in the non-inhibited recordings, the possible phase preference was studied, and none of the cases showed a non-uniform phase distribution after electrical stimulation (Fig. 6*F*; Rayleigh value > 0.05 in all cases).

Discussion

Brain oscillations have been reliably proposed as a substrate for effective communication among multiple brain regions. In particular, theta oscillations have been linked to information processing in the hippocampus, a structure known to play a key role in episodic memory and spatial information (Fries *et al.* 2001; Hasselmo *et al.* 2002; Buzsáki, 2006). However, it has been well documented that MS/DBv is a key subcortical node for hippocampal theta rhythmicity generation (Gogolák *et al.* 1968; Gaztelu & Buño, 1982; Stewart & Fox, 1990; Vinogradova, 1995; Brazhnik & Fox, 1997; Vertes & Kocsis, 1997; Wang, 2002). Both structures generally constitute the septohippocampal complex, which is responsible for the theta state.

Multiple theta oscillators have been reported as nodes coupled to the septohippocampal system (Vertes *et al.* 2004, for a review). Theta rhythmic neuronal activity has been described in a number of brainstem areas that belong to the ascending brainstem–hippocampal axis (Vertes & Kocsis, 1997). One of our previous studies described the existence of a salient theta oscillator in the pontine NI, which became synchronous with the hippocampal theta rhythm (Cervera-Ferri *et al.* 2011). Although a relationship between theta oscillations and specific brainstem reticular formation areas has been widely accepted, research on its dynamics deserves special attention.

Our results corroborate the existence of flows of information as codes between NI neurons and the septohippocampal complex within theta oscillations. The NI is organised in three functional groups of neurons, whose firing patterns change in correlation with the presence of theta rhythmicity in the hippocampus, which achieves a high degree of coupling between both structures (Martínez-Bellver *et al.* 2015). We here report results that validate the interdependence between the activities of both the NI and hippocampus under theta frequencies. Given these observations, it is of interest to determine whether this increased information within theta ranges can be attributable to a leading direction between both sources.

Granger causality has become an increasingly popular analysis method, thanks to its many successful applications in very different knowledge fields (Ding *et al.* 2006; Bressler *et al.* 2008; Deshpande *et al.* 2010; Hwang *et al.* 2010; Schippers *et al.* 2010; Bressler & Seth, 2011; Jiao *et al.* 2011; Luo *et al.* 2011; Ge *et al.* 2012). This approach is efficient for assessing the effective directional coupling of signals sourced from a set of interconnected nodes (Granger, 1969; Ding *et al.* 2006; Seth & Edelman, 2007). Here we used Granger causality to test the hypothesis that the coupled activities between both areas showed a preferential causal relation.

Our findings lead to the conclusion that a significant bidirectional influence exists between the NI and the hippocampus on the theta state elicited by sensory activation (tail pinch), where the NI→HPC flow predominated, and that this asymmetry could be well differentiated in all three neuronal groups described in the NI. Thus under spontaneous conditions, the hippocampal field potential seemed independent of NI neurons with periods of uncoupled activity. Only when a clear theta oscillation predominated in the hippocampus could a defined directionality in the oscillatory patterns of both areas be assigned.

The finding that the spike train of type III neurons at theta frequencies contained information capable of predicting future oscillatory patterns in the septohippocampal system during theta-evoked rhythmicity is particularly interesting. These neurons, which are virtually silent under control conditions, fire rhythmically within the theta range coupled to hippocampal oscillation (Martínez-Bellver *et al.* 2015). In this context, we also found in the present work a minor proportion of periods during which the activity recorded in type III neurons could be predicted from the preceding signal captured in the hippocampus. In contrast, a descending signal from the hippocampus mostly preceded the activity of types I and II NI neurons, but within the 10–20 Hz range of frequencies, which led to their particular firing rates going beyond the theta band. These findings suggest that with sensory activation, an ascending input from the NI, led by type III neurons, effectively drove the septohippocampal system in theta coding. However, these prone epochs alternated with short hippocampal theta rhythm periods to recruit NI neurons. Furthermore, the different populations of neurons in the NI displayed a distinct preponderance of directionality.

Our results can be integrated into the multi-synaptic connectivity between both the NI and the hippocampus. The NI forms part of a distributed complex network, whose nodes are related directly with hippocampal activation. In particular, early works demonstrated the existence of an ascending projection from the NI to the main subcortical and brainstem nuclei involved in driving theta rhythmicity in the hippocampus, including median raphe and interpeduncular nuclei, and the supramammillary nucleus (Goto *et al.* 2001; Olucha-Bordonau *et al.* 2003; Teruel-Martí *et al.* 2008). This ascending pathway is ultimately relayed in the MS/DBv complex, a previous node to the hippocampal target. Moreover, NI is the main relay between RPO and the MS/DBv, activator and pacemaker of the theta rhythm, respectively

(Teruel-Martí *et al.* 2008). A recent report about bidirectional connectivity between the septal area and the NI has described a major ascending projection from the NI to MS/DBv, which is complemented with a minor reciprocal descending pathway (Sánchez-Pérez *et al.* 2015). This asymmetrical loop could assume the anatomical substrate of the functional data described in our results. Whereas type III neurons would mostly be the substrate of the ascending projection, types I and II would be good candidates as the main septal descending pathway target.

Taken together, these data confer a new level of explanation to the coupled theta status between the NI and the hippocampus under sensory activation. In this situation, our analysis reflected a close dynamical brainstem–hippocampus loop, understood as the causal influences that the neuronal populations in one brain area exert on those in another. Given the pattern of theta oscillations, both areas maintained bidirectional coupling with a predominant ascending flow, together with accompanying short epochs in the reversal causal directionality. Flow alternation dynamics could be coupled to the micro-perturbations of ongoing theta. This idea suggests the potential role of the NI as an active actor in the theta state, and not as a strict driver or initiator of hippocampal rhythmicity.

An open question remains: how do these neuronal populations interact? The second part of our work was devoted to evidencing a phase shift or reset of hippocampal theta waves elicited by electrical pulses on the NI. As described above, hippocampal oscillation showed a constant phase immediately after the stimulus was applied to the NI, which was independent of the pre-stimulus phase. We further hypothesised that MS/DBv could be the node by which NI stimulation evoked this phase resetting. Accordingly, no theta reset evidence appeared in our experiments when the MS/DBv complex was deactivated. Many works have previously confirmed that the electrical stimulation of the medial septal area (Buño *et al.* 1978; García-Sánchez *et al.* 1978) is capable of resetting the hippocampal theta. This is also true, even for part of its afferences, including the reticular formation (Gaztelu & Buño, 1982) and the medial forebrain bundle (Brazhnik & Vinogradova, 1988). Gaztelu & Buño (1982) proved that the hippocampal theta reset was caused by fitting the MS/DBv phase. These authors described septal type 1 neurons, defined as 'pacemaker' cells of hippocampal theta rhythmicity, which were responsible for evoking a phase reset on the theta band. These data suggest that the phase shift that we elicited with NI stimulation necessarily involves the septal area. Accordingly, the septal inhibition results of our study corroborated that MS/DBv was a node required to initiate a theta episode in the hippocampus. On the whole, we believe that the type III neurons of the NI are able to activate septal type 1 neurons and, therefore, trigger a theta period, which begins by a phase reset.

Furthermore, it has been recently proved that optogenetic activation of the parvalbumin neurons (PV) in MS/DBv evokes a rhythmic feedback with hippocampal circuits contributing to initiation and maintenance of the theta oscillations (Vandecasteele *et al.* 2014; Bender *et al.* 2015). In these works, it is worth noting that stimulation pulses over septal PV neurons are able to reset the theta phase, adjusting the frequency of the ongoing theta waves of the hippocampus. Accordingly, it has been shown that the septal PV population is targeted by direct projections arising from NI (Olucha-Bordonau *et al.* 2012). Both results are consistent with the idea that the NI is able to elicit theta oscillation using the MS/DBv area as a key node, where septal PV neurons trigger new theta epochs in the hippocampal activity by a phase reset mechanism.

The neurochemical phenotype of the NI is characterised by a variety of neurotransmitters and neuromodulators, including neurotensin, cholecystokinin, and ranatensin, relaxin-3 and glutamate (Jennes *et al.* 1982; Chronwall *et al.* 1985*a*,*b*; Olucha-Bordonau *et al.* 2003; Tanaka *et al.* 2005; Ma *et al.* 2007; Cervera-Ferri *et al.* 2012). However, the presence of GABA markers within the NI (glutamic acid decarboxylase and calcium-binding proteins calretinin and calbindin) indicates various inhibitory neuronal populations, some of which turn out to be ascending projection neurons with the target in the MS/BDv, among others (Goto *et al.* 2001; Olucha-Bordonau *et al.* 2003). This inhibitory input over the MS/BDv is in accordance with the model proposed by Denham and Borisyuk (2000), in which a direct inhibitory input to the medial septum serves to synchronise the rhythmic discharge of the septal neurons 'by a reset' mechanism. This theta rhythm production model describes a hippocampal-–septal loop in which theta waves are sustained by means of a resetting process. Therefore, the NI inhibitory input over the septohippocampal system could explain the onset of a theta cycle.

The hippocampal theta reset has been found to follow stimulus presentations or the electrical stimulation of afferent pathways (Brazhnik *et al.* 1985; Vinogradova *et al.* 1993; Givens, 1996; Tesche & Karhu, 2000; Williams & Givens, 2003). The functional significance of theta reset herein described is not obvious. However, the phase resetting of neural oscillations, which provide temporal windows for cognitive processing, is a general mechanism involved in optimal information encoding (Canavier, 2015). Theta reset has been proposed as a mechanism for phase-locking hippocampal activity to relevant events and could, therefore, enhance cognitive processing (Givens, 1996; Hasselmo, 2007, 2008). Resetting theta waves may enhance cognitive processing, in which theta waves become phase-locked to incoming sensory stimuli (Adey, 1967; Givens, 1996; Vinogradova *et al.* 1996). Moreover, synaptic plasticity is facilitated by theta wave reset when creating optimal conditions for the long-term potentiation

of relevant stimuli (McCartney *et al.* 2004). Thus our results indicate that NI could be considered a relevant node to drive theta activity in the presence of salient events, as evidenced by sensory stimulation. Accordingly, its sensitivity to CRH makes the NI responsive to stress and arousal (Potter *et al.* 1994; Bittencourt & Sawchenko, 2000, Goto *et al.* 2001; Banerjee *et al.* 2010). This neurochemical feature allows the suggestion that the NI could reset theta oscillations in response to highly arousing stimuli, and could thus provide hippocampal processing with an optimal temporal framework under certain conditions.

In summary, the rat model of hippocampal theta rhythmicity, in parallel with multichannel recordings, provides a useful experimental platform to perform causal analyses that tests the presence of hierarchical nodes inside the whole network that underlies theta oscillations. Our analyses suggest specific directional patterns and putative looping between the NI and the hippocampus, with a bottom–top directionality that predominates in the theta state (Fig. 7). The high level of communication between both areas with sensory stimulation could imply reciprocal top–bottom connectivity, whose aim is to ensure high coupling values. Our data further indicated that the brainstem-evoked theta onset in the hippocampus began with the phase resetting of theta waves as a way to initiate new hippocampal processing. While the present results are compelling, they also reinforce the need to carry out further experiments, including use of extra recording sites, to better analyse the dynamics and causal relationships in the complete theta network.
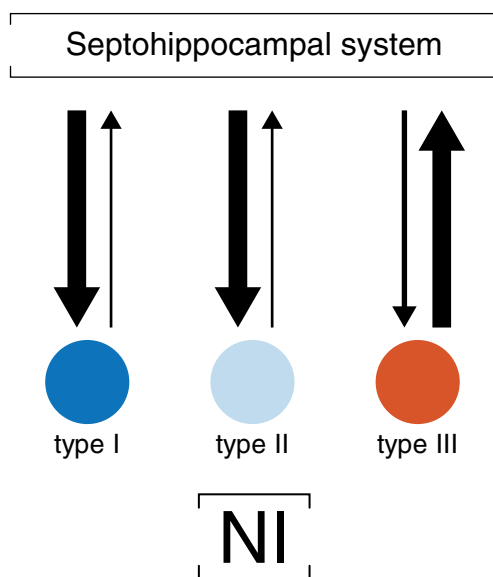
Figure 7. Schematic diagram of the causal interactions among the NI neurons and the septo-hippocampal system
Arrow thickness reflects the main causal flow during hippocampal theta periods. [Colour figure can be viewed at wileyonlinelibrary.com]

References

Adey WR (1967). Hippocampal states and functional relations with corticosubcortical systems in attention and learning. *Progr Brain Res* **27**, 228–245.

Alonso A & García-Austt E (1987*a*). Neuronal sources of theta rhythm in the entorhinal cortex of the rat. I. Laminar distribution of theta field potentials. *Exp Brain Res* **67**, 493–501.

Alonso A & García-Austt E (1987*b*). Neuronal sources of theta rhythm in the entorhinal cortex of the rat. II. Phase relations between unit discharges and theta field potentials. *Exp Brain Res* **67**, 502–509.

Alonso A, Khateb A, Fort P, Jones BE & Mühlethaler M (1996). Differential oscillatory properties of cholinergic and noncholinergic nucleus basalis neurons in guinea pig brain slice. *The Eur J Neurosci* **8**, 169–182.

Banerjee A, Shen PJ, Ma S, Bathgate RAD & Gundlach AL (2010). Swim stress excitation of nucleus incertus and rapid induction of relaxin-3 expression via CRF1 activation. *Neuropharmacology* **58**, 145–155.

Bassant MH & Poindessous-Jazat F (2001). Ventral tegmental nucleus of Gudden: a pontine hippocampal theta generator? *Hippocampus* **11**, 809–813.

Bender F, Gorbati M, Cadavieco MC, Denisova N, Gao X, Holman C, Korotkova T & Ponomarenko A (2015). Theta oscillations regulate the speed of locomotion via a hippocampus to lateral septum pathway. *Nat Commun* **6**, 8521.

Bittencourt JC & Sawchenko PE (2000). Do centrally administered neuropeptides access cognate receptors?: An analysis in the central corticotropin-releasing factor system. *J Neurosci* **20**, 1142–1156.

Bland BH (1986). The physiology and pharmacology of hippocampal formation theta rhythms. *Prog Neurobiol* **26**, 1–54.

Bland BH & Oddie SD (1998). Anatomical, electrophysiological and pharmacological studies of ascending brainstem hippocampal synchronizing pathways. *Neurosci Biobehav Rev* **22**, 259–273.

Brankack J, Seidenbecher T & Müller-Gärtner HW (1996). Task-relevant late positive component in rats: is it related to hippocampal theta rhythm? *Hippocampus* **6**, 475–482.

Brazhnik ES & Vinogradova OS (1988). Modulation of the afferent input to the septal neurons by cholinergic drugs. *Brain Res* **451**, 1–12.

Brazhnik ES, Vinogradova OS & Karanov AM (1985). Frequency modulation of neuronal theta-bursts in rabbit's septum by low-frequency repetitive stimulation of the afferent pathways. *Neuroscience* **14**, 501–508.

Brazhnik ES & Fox SE (1997). Intracellular recordings from medial septal neurons during hippocampal theta rhythm. *Exp Brain Res* **114**, 442–453.

Bressler SL & Seth AK (2011). Wiener-Granger causality: a well-established methodology. *Neuroimage* **58**, 323–329.

Bressler SL, Tang W, Sylvester CM, Shulman GL & Corbetta M (2008). Top-down control of human visual cortex by frontal and parietal cortex in anticipatory visual spatial attention. *J Neurosci* **28**, 10056–10061.

Buño W, Garcia-Sanchez JL & Garcia-Austt E (1978). Reset of hippocampal rhythmical activities by afferent stimulation. *Brain Res Bull* **3**, 21–28.

Buzsáki G (2002). Theta oscillations in the hippocampus. *Neuron* **33**, 325–340.

Buzsáki G (2005). Theta rhythm of navigation: link between path integration and landmark navigation, episodic and semantic memory. *Hippocampus* **15**, 827–840.

Buzsáki G (2006). *Rhythms of the Brain.* Oxford University Press, New York.

Canavier CC (2015). Phase-resetting as a tool of information transmission. *Curr Opin Neurobiol* **31**, 206–213.

Cervera-Ferri A, Guerrero-Martínez J, Bataller-Mompeán M, Taberner-Cortes A, Martínez-Ricós J, Ruiz-Torner A & Teruel-Martí V (2011). Theta synchronization between the hippocampus and the nucleus incertus in urethane-anaesthetized rats. *Exp Brain Res* **211**, 177–192.

Cervera-Ferri A, Rahmani Y, Martínez-Bellver S, Teruel-Martí V & Martínez-Ricós J (2012). Glutamatergic projection from the nucleus incertus to the septohippocampal system. *Neurosci Lett* **517**, 71–76.

Chalmers DT, Lovenberg TW & De Souza EB (1995). Localization of novel corticotropin-releasing factor receptor (CRF2) mRNA expression to specific subcortical nuclei in rat brain: comparison with CRF1 receptor mRNA expression. *J Neurosci* **15**, 6340–6350.

Chronwall BM, DiMaggio DA, Massari VJ, Pickel VM, Ruggiero DA & O'Donohue TL (1985). The anatomy of neuropeptide-Y-containing neurons in rat brain. *Neuroscience* **15**, 1159–1181.

Chronwall BM, Skirboll LR & O'Donohue TL (1985). Demonstration of a pontine-hippocampal projection containing a ranatensin-like peptide. *Neurosci Lett* **53**, 109–114.

Denham MJ & Borisyuk RM (2000). A model of theta rhythm production in the septal-hippocampal system and its modulation by ascending brain stem pathways. *Hippocampus* **10**, 698–716.

Deshpande G, Sathian K & Hu X (2010). Effect of hemodynamic variability on Granger causality analysis of fMRI. *Neuroimage* **52**, 884–896.

Ding L, Worrell GA, Lagerlund TD & He B (2006). Spatio-temporal source localization and Granger causality in ictal source analysis. *Conf Proc IEEE Eng Med Biol Soc* **1**, 3670–3671.

Faris PD & Sainsbury RS (1990). The role of the pontis oralis in the generation of RSA activity in the hippocampus of the guinea pig. *Physiol Behav* **47**, 1193–1199.

Foster DJ & Wilson MA (2006). Reverse replay of behavioural sequences in hippocampal place cells during the awake state. *Nature* **440**, 680–683.

Freiwald WA, Valdes P, Bosch J, Biscay R, Jimenez JC, Rodriguez LM & Singer W (1999). Testing non-linearity and directedness of interactions between neural groups in the macaque inferotemporal cortex. *J Neurosci Methods* **94**, 105–119.

Fries P, Reynolds JH, Rorie AE & Desimone R (2001). Modulation of oscillatory neuronal synchronization by selective visual attention. *Science* **291**, 1560–1563.

García-Sánchez JL, Buño W, Fuentes J & García-Austt E (1978). Non-rhythmical hippocampal units, theta rhythm and afferent stimulation. *Brain Res Bull* **3**, 213–219.

Gaztelu JM & Buño W (1982). Septo-hippocampal relationships during EEG theta rhythm. *Electroencephalogr Clin Neurophysiol* **54**, 375–387.

Ge T, Feng J, Grabenhorst F & Rolls ET (2012). Componential Granger causality, and its application to identifying the source and mechanisms of the top-down biased activation that controls attention to affective vs sensory processing. *Neuroimage* **59**, 1846–1858.

Givens B (1996). Stimulus-evoked resetting of the dentate theta rhythm: relation to working memory. *Neuroreport* **8**, 159–163.

Gogolák G, Stumpf C, Petsche H & Sterc J (1968). The firing pattern of septal neurons and the form of the hippocampal theta wave. *Brain Res* **7**, 201–207.

Goto M, Swanson LW & Canteras NS (2001). Connections of the nucleus incertus. *J Comp Neurol* **438**, 86–122.

Granger CWJ & Aug N (1969). Investigating causal relations by econometric models and cross-spectral methods. *Econometrica* **37**, 424–438.

Grástyan E, Lissak K, Madarasz I & Donhoffer H (1959). Hippocampal electrical activity during the development of conditioned reflexes. *Electroencephalogr Clin Neurophysiol* **11**, 409–430.

Green J & Arduini A (1954). Hippocampal electrical activity in arousal. *J Neurophysiol* **17**, 533–557.

Hasselmo ME (2007). Arc length coding by interference of theta frequency oscillations may underlie context-dependent hippocampal unit data and episodic memory function. *Learn Mem* **14**, 782–794.

Hasselmo M (2008). Temporally structured replay of neural activity in a model of entorhinal cortex, hippocampus and postsubiculum. *Eur J Neurosci* **28**, 1301–1315.

Hasselmo ME, Bodelón C & Wyble BP (2002). A proposed function for hippocampal theta rhythm: separate phases of encoding and retrieval enhance reversal of prior learning. *Neural Comput* **14**, 793–817.

Huerta PT & Lisman JE (1995). Bidirectional synaptic plasticity induced by a single burst during cholinergic theta oscillation in CA1 in vitro. *Neuron* **15**, 1053–1063.

Hwang K, Velanova K & Luna B (2010). Strengthening of top-down frontal cognitive control networks underlying the development of inhibitory control: a functional magnetic resonance imaging effective connectivity study. *J Neurosci* **30**, 15535–15545.

Jennes L, Stumpf WE & Kalivas PW (1982). Neurotensin: topographical distribution in rat brain by immunohistochemistry. *J Comp Neurol* **210**, 211–224.

Jiao Q, Lu G, Zhang Z, Zhong Y, Wang Z, Guo Y & Liu Y (2011). Granger causal influence predicts BOLD activity levels in the default mode network. *Hum Brain Mapp* **32**, 154–161.

Jouvet M (1969). Biogenic amines and the states of sleep. *Science* **163**, 32–41.

Kamiński MJ & Blinowska KJ (1991). A new method of the description of the information flow in the brain structures. *Biol Cybern* **65**, 203–210.

Kamiński M, Ding M, Truccolo W & Bressler SL (2001). Evaluating causal relations in neural systems: Granger causality, directed transfer function and statistical assessment of significance. *Biol Cybern* **85**, 145–157.

Kirk IJ & McNaughton N (1991). Supramammillary cell firing and hippocampal rhythmical slow activity. *Neuroreport* **2**, 723–725.

Kirk IJ, Oddie SD, Konopacki J & Bland BH (1996). Evidence for differential control of posterior hypothalamic, supramammillary, and medial mammillary theta-related cellular discharge by ascending and descending pathways. *J Neurosci* **16**, 5547–5554.

Kocsis B & Vertes RP (1996). Midbrain raphe cell firing and hippocampal theta rhythm in urethane-anaesthetized rats. *Neuroreport* **7**, 2867–2872.

Leung LW (1985). Spectral analysis of hippocampal EEG in the freely moving rat: effects of centrally active drugs and relations to evoked potentials. *Electroencephalogr Clin Neurophysiol* **60**, 65–77.

Liu Y, San Liang X & Weisberg RH (2007). Rectification of the bias in the wavelet power spectrum. *J Atmos Oceanic Technol* **24**, 2093–2102.

Luo Q, Ge T & Feng J (2011). Granger causality with signal-dependent noise. *Neuroimage* **57**, 1422–1429.

Ma S, Blasiak A, Olucha-Bordonau FE, Verberne AJM & Gundlach AL (2013). Heterogeneous responses of nucleus incertus neurons to corticotrophin-releasing factor and coherent activity with hippocampal theta rhythm in the rat. *J Physiol* **591**, 3981–4001.

Ma S, Bonaventure P, Ferraro T, Shen PJ, Burazin TCD, Bathgate RAD, Liu C, Tregear GW, Sutton SW & Gundlach AL (2007). Relaxin-3 in GABA projection neurons of nucleus incertus suggests widespread influence on forebrain circuits via G-protein-coupled receptor-135 in the rat. *Neuroscience* **144**, 165–190.

Martínez-Bellver S, Cervera-Ferri A, Martínez-Ricós J, Ruiz-Torner A, Luque-García A, Blasco-Serra A, Guerrero-Martínez J, Bataller-Mompeán M & Teruel-Martí V (2015). Regular theta-firing neurons in the nucleus incertus during sustained hippocampal activation. *Eur J Neurosci* **41**, 1049–1067.

McCartney H, Johnson AD, Weil ZM & Givens B (2004). Theta reset produces optimal conditions for long-term potentiation. *Hippocampus* **14**, 684–687.

Mitchell SJ & Ranck JB (1980). Generation of theta rhythm in medial entorhinal cortex of freely moving rats. *Brain Res* **189**, 49–66.

Niso G, Bruña R, Pereda E, Gutiérrez R, Bajo R, Maestú F & del-Pozo F (2013). HERMES: towards an integrated toolbox to characterize functional and effective brain connectivity. *Neuroinformatics* **11** 405–434.

Nuñez A, Cervera-Ferri A, Olucha-Bordonau F, Ruiz-Torner A & Teruel V (2006). Nucleus incertus contribution to hippocampal theta rhythm generation. *Eur J Neurosci* **23**, 2731–2738.

O'Keefe J & Recce ML (1993). Phase relationship between hippocampal place units and the EEG theta rhythm. *Hippocampus* **3**, 317–330.

Olucha-Bordonau FE, Teruel V, Barcia-González J, Ruiz-Torner A, Valverde-Navarro AA & Martínez-Soriano F (2003). Cytoarchitecture and efferent projections of the nucleus incertus of the rat. *J Comp Neurol* **464**, 62–97.

Olucha-Bordonau FE, Otero-García M, Sánchez-Pérez AM, Núñez A, Ma S & Gundlach AL (2012). Distribution and targets of the relaxin-3 innervation of the septal area in the rat. *J Comp Neurol* **520**, 1903–1939.

O'Neill J, Senior TJ, Allen K, Huxter JR & Csicsvari J (2008). Reactivation of experience-dependent cell assembly patterns in the hippocampus. *Nat Neurosci* **11**, 209–215.

Paxinos G & Watson C (2004). *The Rat Brain in Stereotaxic Coordinates: The New Coronal Set.* Academic Press, San Diego.

Pignatelli M, Beyeler A & Leinekugel X (2012). Neural circuits underlying the generation of theta oscillations. *J Physiol Paris* **106**, 81–92.

Potter E, Behan DP, Linton EA, Lowry PJ, Sawchenko PE & Vale WW (1992). The central distribution of a corticotropin-releasing factor (CRF)-binding protein predicts multiple sites and modes of interaction with CRF. *Proc Natl Acad Sci USA* **89**, 4192–4196.

Potter E, Sutton S, Donaldson C, Chen R, Perrin M, Lewis K & Vale W (1994). Distribution of corticotropin-releasing factor receptor mRNA expression in the rat brain and pituitary. *Proc Natl Acad Sci USA* **91**, 8777–8781.

Sánchez-Pérez AM, Arnal-Vicente I, Santos FN, Pereira CW, ElMlili N, Sanjuan J & Olucha-Bordonau FE (2015). Septal projections to nucleus incertus in the rat: bidirectional pathways for modulation of hippocampal function. *J Comp Neurol* **523**, 565–588.

Schippers MB, Roebroeck A, Renken R, Nanetti L & Keysers C (2010). Mapping the information flow from one brain to another during gestural communication. *Proc Natl Acad Sci USA* **107**, 9388–9393.

Seth AK (2010). A MATLAB toolbox for Granger causal connectivity analysis. *J Neurosci Methods* **186**, 262–273.

Seth AK & Edelman GM (2007). Distinguishing causal interactions in neural populations. *Neural Comput* **19**, 910–933.

Shannon CE (1948). A mathematical theory of communication. *Bell Syst Tech J* **27**, 379–423.

Singer W (1999). Neuronal synchrony: A versatile code for the definition of relations? *Neuron*, **24**, 49–65.

Stewart M & Fox SE (1990). Firing relations of lateral septal neurons to the hippocampal theta rhythm in urethane anaesthetized rats. *Exp Brain Res* **79**, 92–96.

Szucs A (1998) Applications of the spike density function in analysis of neuronal firing patterns. *J Neurosci Methods* **81**, 159–167.

Tanaka M, Iijima N, Miyamoto Y, Fukusumi S, Itoh Y, Ozawa H & Ibata Y (2005) Neurons expressing relaxin 3/INSL 7 in the nucleus incertus respond to stress. *Eur J Neurosci* **21**, 1659–1670.

Teruel-Martí V, Cervera-Ferri A, Nuñez A, Valverde-Navarro AA, Olucha-Bordonau FE & Ruiz-Torner A (2008). Anatomical evidence for a ponto-septal pathway via the nucleus incertus in the rat. *Brain Res* **1218**, 87–96.

Tesche CD & Karhu J (2000). Theta oscillations index human hippocampal activation during a working memory task. *Proc Natl Acad Sci USA* **97**, 919–924.

Torrence C & Compo GP (1998). A practical guide to wavelet analysis. *B Am Meteorol Soc* **79**, 61–78.

Vandecasteele M, Varga V, Berényi A, Papp E, Barthó P, Venance L, Freund TF & Buzsáki G (2014). Optogenetic activation of septal cholinergic neurons suppresses sharp wave ripples and enhances theta oscillations in the hippocampus. *Proc Natl Acad Sci USA* **111**, 13535–13540.

Vanderwolf C (1969). Hippocampal electrical activity and voluntary movement in the rat. *Electroencephalogr Clin Neurophysiol* **26**, 407–418.

Vertes RP, Hoover WB & Viana Di Prisco G. (2004). Theta rhythm of the hippocampus: subcortical control and functional significance. *Behav Cogn Neurosci Rev* **3**, 173–200.

Vertes R & Kocsis B (1997). Brainstem-diencephalo-septohippocampal systems controlling the theta rhythm of the hippocampus. *Neuroscience* **81**, 893–926.

Vinogradova OS (1995). Expression, control, and probable functional significance of the neuronal theta-rhythm. *Prog Neurobiol* **45**, 523–583.

Vinogradova OS, Brazhnik ES, Kichigina VF & Stafekhina VS (1993). Theta modulation of neurons of the hippocampus of the rabbit and its interrelationship with other parameters of spontaneous and evoked activity. *Neurosci Behav Physiol* **23**, 226–239.

Vinogradova OS, Brazhnik ES, Kichigina VF & Stafekhina VS (1996). Modulation of the reaction of hippocampal neurons to sensory stimuli by cholinergic substances. *Neurosci Behav Physiol* **26**, 113–124.

Wang XJ (2002). Pacemaker neurons for the theta rhythm and their synchronization in the septohippocampal reciprocal loop. *J Neurophysiol* **87**, 889–900.

Williams J & Givens B (2003). Stimulation-induced reset of hippocampal theta in the freely performing rat. *Hippocampus* **13**, 109–116.

Young CK & McNaughton N (2009). Coupling of theta oscillations between anterior and posterior midline cortex and with the hippocampus in freely behaving rats. *Cereb Cortex* **19**, 24–40.

Additional information

Competing interests

The authors declare no competing financial interests.

Author contributions

Funding

Acknowledgements